IOPscience iopscience.iop.org

Home Search Collections Journals About Contact us My IOPscience

Stokes and anti-Stokes resonant Raman scattering of $F_H(CH^-)$ defects in CsBr

This article has been downloaded from IOPscience. Please scroll down to see the full text article.

1989 J. Phys.: Condens. Matter 1 3239

(http://iopscience.iop.org/0953-8984/1/20/005)

View the table of contents for this issue, or go to the journal homepage for more

Download details:
IP Address: 94.79.44.176
The article was downloaded on 10/05/2010 at 18:11

Please note that terms and conditions apply.

J. Phys.: Condens. Matter **1** (1989) 3239–3252. Printed in the UK

Stokes and anti-Stokes resonant Raman scattering of $F_H(CN^-)$ defects in CsBr

G Cachei†, H Stolz†, W von der Osten† and Fritz Lüty‡

† Fachbereich Physik, Universität-GH, D-4790 Paderborn, Federal Republic of Germany

‡ Physics Department, University of Utah, Salt Lake City, UT 84112, USA

Received 22 August 1988

Abstract. Association of F centres with CN^- molecular ions in CsBr forms $F_H(CN^-)$ complexes with electronic absorption bands at 1.78 eV ($F_H(1)$) and 1.94 eV ($F_H(2)$). Using continuous-wave excitation in resonance with these absorptions, we studied Stokes and anti-Stokes Raman scattering at low temperature to investigate the F-centre/CN^- coupling and the recently observed electronic–vibrational energy transfer by which excited states of the CN^- stretching mode become populated. $F_H(1)$ and $F_H(2)$ excited anti-Stokes spectra show distinct differences in scattered intensity and number of Raman lines, suggesting different coupling strengths and timescales for the corresponding transfer processes. The dependence of the spectra on light polarisation, excitation power and sample temperature is studied and discussed with regard to defect symmetry and relative population of states. The quadratic dependence of scattered intensity on excitation power observed at lowest power level is consistent with a two-step nature of the observed processes, involving population of vibrational states and scattering from these. Owing to the good resolution, the spectra can be analysed in terms of isotope effects on the CN^- stretching-mode energy. Preliminary measurements of the lattice phonon and local-mode Raman spectra show that further refinements of the model are required.

1. Introduction

The $F_H(CN^-)$ defect in the body-centred cubic caesium halides is assumed to consist of an F-centre/CN^- molecule pair along a $\langle 100 \rangle$ crystal axis [1]. The attached CN^- reduces the local symmetry of the F centre and, because of the interaction, splits the F absorption into two separate transitions, $F_H(1)$ and $F_H(2)$, which predominantly absorb parallel and perpendicular to the pair axis. Compared with the well known F_A centre (an F centre associated with an alkali-ion impurity) [2], the most exciting feature of this novel type of aggregate centre originates from the additional vibrational degree of freedom introduced by the molecule. As observed for the first time for an F-centre/CN^- defect pair in KCl [3], energy transfer occurs from the optically excited F centre to the CN^- internal stretching mode, which then produces vibrational emission in the 5 μm range. In KCl this transfer turned out to be merely weak, a fact obviously correlated with the small change in the F absorption and emission band shape and position following the F-centre/CN^- aggregation. This situation changes dramatically in caesium halides, where the F centre seems to be much more strongly coupled to the CN^- molecular ion. Pumping in the $F_H(CN^-)$ electronic absorption, e.g. in CsCl and CsBr, was found to give intense

0953-8984/89/203239 + 14 $02.50 © 1989 IOP Publishing Ltd

CN^- vibrational emission with high quantum and energy conversion efficiency [1, 4]. The excitation and de-excitation cycle efficiently populates excited vibrational states from which $\Delta v = -1$ luminescence transitions between adjacent levels (with quantum numbers v) occur to give a nearly equidistant spectrum. This consists of several lines shifted with respect to each other by the anharmonicity of the stretching vibration.

We report here results of resonant Raman scattering, which besides infrared emission spectroscopy, is an extremely powerful technique to study this highly interesting phenomenon. The population of excited vibrational states will give rise not only to Stokes but also to anti-Stokes scattering, both strongly enhanced through resonance Raman observation. In addition, the spectra are transferred into the visible, with the advantage that highly sensitive signal detection may be employed. In our measurements we used continuous laser excitation, which, in contrast to previous anti-Stokes studies of $F_H(CN^-)$ centres in CsCl under pulsed excitation [5], allows considerably improved spectral resolution to reveal fine details in the spectra. In addition, we are also able to measure Stokes spectra by which, in contrast to anti-Stokes Raman scattering and infrared vibrational luminescence, the population of the vibrational ground state $v = 0$ can be revealed for the first time and may be compared to the excited-states populations.

For our study of resonant Raman scattering from $F_H(CN^-)$ defects we have chosen CsBr, which in comparison with other caesium halides exhibits several advantages. In contrast to CsCl, which has a troublesome structural phase transition around 827 K, good-quality oriented single crystals of CsBr can be grown and additively coloured close to the melting point without problems. On the other hand, as implied by the magnitude of the $F_H(1)$–$F_H(2)$ band energy splitting, the perturbation of the F centre by the attached CN^- ion in this material is strong and much larger than in CsI, although weaker than in CsCl. From this we anticipated strong interaction between the F-centre electron and the CN^- vibrational states, so that efficient energy transfer into the CN^- stretching mode and therefore drastic effects on the resonant Raman spectrum may be expected.

2. Experimental techniques

We have used several oriented samples, which were cut from a CsBr single crystal grown by the Czochralski method at the Crystal Growth Laboratory of the University of Utah. They were doped with nominally 1% mole fraction CsCN. To produce the necessary F centres, the samples were additively coloured in the usual way in potassium vapour at 793 K, with the crystal held at 823 K and quickly quenched after that to room temperature to avoid unwanted F-centre aggregation. After final polishing, the crystal was immediately mounted in a variable-temperature cryostat. Special care was taken to keep the sample in the dark during all handling. The low-temperature absorption spectrum at this stage essentially showed the well known F band with its characteristic spectral substructure due to spin–orbit effects and phonon coupling (for references see e.g. [6]). At 165 K, irradiation of the sample with moderate F-band light from two opposite sides for 10 to 15 min each induces the F-centre/CN^- aggregation process, which was traced by the developing $F_H(CN^-)$ absorption band (figure 1). In the case of strong F absorption, additional F light irradiation by a defocused laser beam from below was used to reinforce aggregation and to obtain a more homogeneous centre distribution throughout the crystal volume. Following aggregation, the crystal was left in the dark for 15 min before cooling down to lower temperature to let an additional absorption band at 1.61 eV decay.

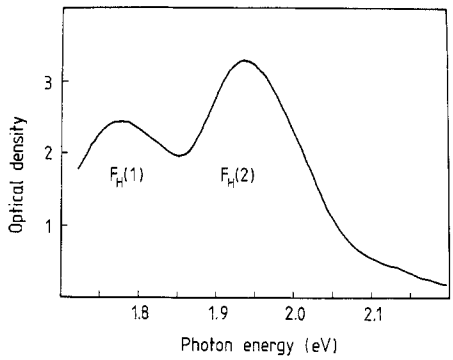

Figure 1. Absorption spectrum of $F_H(CN^-)$ centres in CsBr: $10^{-2}CN^-$ at 5 K. The crystal was additively coloured to contain F centres in an estimated concentration of 10^{17} cm^{-3}, which were then aggregated with CN^- molecular defects.

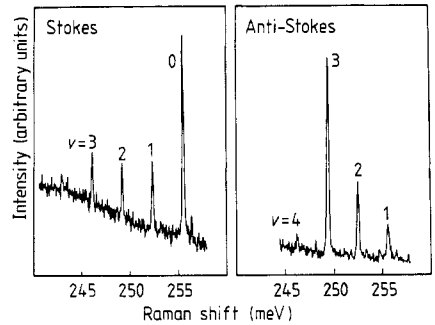

Figure 2. Examples of typical unpolarised Stokes ($v \rightarrow v + 1$) and anti-Stokes ($v \rightarrow v - 1$) Raman spectra at $T = 20$ K resonantly excited in the $F_H(2)$ absorption band at 1.980 eV and 1.960 eV, respectively. The excitation power was 180 mW.

Two types of sample orientation were available: one prepared with six orthogonal {1 0 0} surfaces, the other with two {1 0 0} and four {1 1 0} orthogonal faces. In connection with the 90° scattering geometry employed, these orientations allowed various polarisations of the incident and scattered light relative to the crystal axes. In the case of O_h point symmetry, sometimes referred to later, these geometries allow one to decompose the scattering spectra into individual A_{1g}, E_g or T_{2g} components or combinations of these [7]. Since the material does not cleave, the samples had to be sawn and carefully polished. Sample orientation was achieved by use of the Laue x-ray technique. Typical sample size was around $10 \times 8 \times 3$ mm^3.

Our Raman set-up consisted of an Ar^+-laser-pumped tunable dye laser operated with DCM or Rh 6G as excitation source, a 0.85 m Spex double monochromator and conventional photon counting for detection. If necessary, spectral filters were used between the dye laser and the sample to suppress the luminescence background that originated from the dye laser and sometimes perturbed the Raman spectra. To prevent local heating and destruction of the $F_H(CN^-)$ defects, in some experiments the excitation power was kept below 50 mW, with only gentle beam focusing. The sample temperature could be chosen between 2 and 300 K, and the actual temperatures were presumably higher by several Kelvins than those measured at the sample holder. All spectra were normalised to the incident laser power recorded with a reference diode. The spectral range of our monochromator at the low-energy side was limited to 1.71 eV, not permitting us to measure the Stokes spectra for $F_H(1)$ excitation. By adding a halogen lamp, the $F_H(CN^-)$ absorption spectra could be taken in the same set-up.

3. Experimental results and discussion

To facilitate the following presentation and allow easy comparison of the Raman excitation energies with the defect transitions, we display in figure 1 a typical absorption spectrum of $F_H(CN^-)$ centres in our CsBr samples after F-centre/CN^- aggregation. The separation of the $F_H(1)$ and $F_H(2)$ band maxima (at 1.78 and 1.94 eV, respectively) is 0.16 eV compared to 0.27 eV in CsCl, which is very probably related to the larger lattice

Table 1. Experimental $v = 0 \rightleftarrows 1$ Raman energies $\Delta E(CN^-)$ and $\Delta E(F_H(CN^-))$ of isolated and F-centre perturbed CN^- molecules for various isotope configurations. $h\nu_e$ and χ_e are the harmonic oscillator energy and anharmonicity constant from the analysis of the $F_H(CN^-)$ resonant Raman spectra.

	(*a*) $^{12}C^{14}N^-$	(*b*) $^{13}C^{14}N^-$	(*c*) $^{12}C^{15}N^-$
$\Delta E(CN^-)$ (meV)	256.3	250.8	—
$\Delta E(F_H(CN^-))$ (meV)	255.5	250.3	251.6
$h\nu_e$ (meV)	258.8 ± 0.2	253.4 ± 0.2	254.8 ± 0.2
χ_e (10^{-3})	6.1 ± 0.4	6.0 ± 0.4	6.0 ± 0.4

constant (4.29 Å for CsBr, 4.11 Å for CsCl) and hence smaller coupling between the partners.

Excitation in either absorption band produces a series of nearly equidistant (energy difference 3.1 meV or 25 cm^{-1}) narrow Raman lines that are observed in both the Stokes and anti-Stokes spectra (figure 2). These lines correspond to $\Delta v = \pm 1$ transitions between successive vibrational states of the CN^- internal stretching mode of the CN^- molecule (v = vibrational quantum number) and are shifted relative to each other by anharmonicity. Their occurrence strongly parallels the observation of CN^- vibrational emission in the near-infrared [1, 4], with the spectral positions of corresponding lines measured with the two techniques showing good coincidence. Depending on excitation photon energy, exciting power and sample temperature, up to six Raman lines are observed. The occurrence of the anti-Stokes spectrum and of Stokes processes involving quantum states with $v \geqslant 1$ dramatically demonstrates that excited vibrational states participate in the Raman scattering process. As originally discussed [1], these states are effectively populated by efficient energy transfer between the optically excited F electron and the CN^- vibrational modes. Accordingly the electron rapidly relaxes into the ground state, while a substantial population remains in the vibrational states with relatively long lifetimes of the order of milliseconds. Raman scattering probes this population, giving rise to the observed Stokes and anti-Stokes spectra.

3.1. Spectral analysis and isotope effects

The good spectral resolution of our data allows a detailed analysis of the spectra with regard to anharmonicity of the CN^- vibration and some observed finer spectral features. Employing the simple anharmonic oscillator model [8], which neglects terms higher than quadratic, the energy of a vibrational state with quantum number v is given by

$$E_v = h\nu_e(v + \tfrac{1}{2}) - h\nu_e\chi_e(v + \tfrac{1}{2})^2 + \ldots \qquad v = 0, 1, 2, \ldots \tag{1}$$

resulting in energy differences between successive states of

$$\Delta E_{(v+1)\rightarrow v} = E_{v+1} - E_v = h\nu_e[1 - 2\chi_e(v + 1)]. \tag{2}$$

From all measured Raman transition energies, the anharmonicity constant and the oscillator energy are determined to be $\chi_e = 6.1 \times 10^{-3}$ and $h\nu_e = 258.8$ meV, respectively (see table 1).

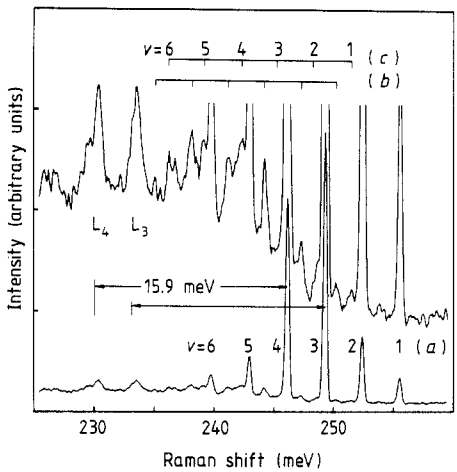

Figure 3. Anti-Stokes Raman spectrum of $F_H(CN^-)$ centres obtained for $F_H(1)$ excitation at $T = 5$ K. Excitation at 1.780 eV with 45 mW laser power. The sequences of lines are $v \rightarrow v - 1$ transitions involving isotopes $^{12}C^{14}N^-$ (*a*), $^{13}C^{14}N^-$ (*b*) and $^{12}C^{15}N^-$ (*c*). L_3 and L_4 are Raman lines due to difference processes involving a 15.9 meV localised phonon.

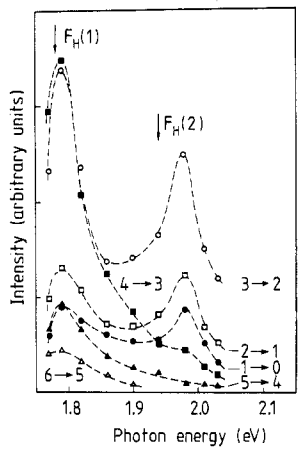

Figure 4. Scattered intensities for various anti-Stokes Raman transitions $v \rightarrow v - 1$ versus excitation photon energy across the $F_H(CN^-)$ absorption at 5 K. Excitation power was 80 mW. The experimental data are corrected for absorption. The arrows mark positions of $F_H(1)$ and $F_H(2)$ band maxima in figure 1.

As illustrated by the anti-Stokes spectrum of figure 3, besides the main series of Raman lines (designated (*a*)) two other much weaker sequences ((*b*) and (*c*)) are observed. Compared to spectrum (*a*), the $v = 1 \rightarrow 0$ transitions are shifted to smaller Raman energies by 5.2 meV (42 cm^{-1}) and 3.9 meV (31 cm^{-1}), respectively. While spectrum (*a*) is due to vibrations of the main isotope $^{12}C^{14}N^-$ coupled to the F centre, the additional sequences (*b*) and (*c*) are associated with the less abundant configurations $^{13}C^{14}N^-$ and $^{12}C^{15}N^-$. The reduced-mass values of these isotope species are larger by 4 and 3% than for $^{12}C^{14}N^-$, leading to smaller vibrational energies. The energetic positions of the Raman lines for the two isotopes, which can be calculated relative to the main $^{12}C^{14}N^-$ series of lines (*a*) from the ratio of reduced masses, agree better than 0.1% with the measured spectral positions. We also calculated the oscillator energies $h\nu_e$ for $^{13}C^{14}N^-$ and $^{12}C^{15}N^-$ (see table 1) and found the anharmonicity constant χ_e to be independent of isotopic composition of the CN^- molecule.

Contrary to the very good agreement regarding isotope effects on the Raman energies, the relative intensities of spectra (*a*) to (*c*) show unexpectedly high deviations compared with the natural relative abundance of isotopes (98.5% : 1.1% : 0.4% for $^{12}C^{14}N^-$: $^{13}C^{14}N^-$: $^{12}C^{15}N^-$). For corresponding transitions we estimate proportions of about 94% : 4% : 2%. In analogy to infrared vibrational luminescence [4, 9], we consider this discrepancy to be due to vibrational energy transfer between vibrationally excited $F_H(CN^-)$ centres. Obviously vibrational energy migrates from F_H centres containing $^{12}C^{14}N^-$ molecules to those with the less abundant species, which have smaller oscillator energies, so that vibrational states of these may become excited even at low temperatures. From the ratio of isolated to F-centre-attached CN^- molecules (about 10^2–10^3, see below) and from the average spacing between the F_H centres, the energy is most

probably transferred via isolated molecules; however, we did not undertake to establish this mechanism in detail.

3.2. Dependence of spectra on excitation photon energy

The assumed axial (C_{4v}) symmetry of the $F_H(CN^-)$ complex, resulting in two different transition moments parallel ($F_H(1)$) and perpendicular ($F_H(2)$) to the centre axis, suggests that the Raman spectra show characteristic variations depending on excitation photon energy and light polarisation. Comparing the anti-Stokes spectra for $F_H(1)$ and $F_H(2)$ excitations, a striking difference between the two lies in the numbers and relative intensities of observed Raman transitions. $F_H(2)$ excitation (figure 2) produces essentially three lines with the $v = 3 \rightarrow 2$ transition being strongest, reflecting efficient electronic–vibrational energy transfer taking place into the $v = 3$ state. In contrast, excitation in the $F_H(1)$ absorption (figure 3) results in up to six Raman lines, revealing preferential population of vibrational states with larger v than for $F_H(2)$ excitation.

To follow the evolution of the spectra between the two situations, we measured the excitation profiles of all anti-Stokes lines across the $F_H(1)$ and $F_H(2)$ absorption bands (figure 4) and found a continuous transition. The most striking effect evident from figure 4 is the drastic reduction of the $v = 4 \rightarrow 3$ line intensity when the excitation energy is tuned from the $F_H(1)$ to the $F_H(2)$ band. It is reduced from its peak value at $F_H(1)$ to only about 5% on the high-energy side of the $F_H(2)$ band, becoming much less intense there than all transitions involving lower quantum states ($v = 1 \rightarrow 0, 2 \rightarrow 1, 3 \rightarrow 2$). Contrary to these transitions, no maximum in scattered intensity appears for the $4 \rightarrow 3$ line in the $F_H(2)$ energy range. For those anti-Stokes lines showing resonance in this range, the maximum of the scattered intensity does not coincide with the $F_H(2)$ band maximum but rather is shifted by about 40 meV to higher energy. This is reminiscent of the Raman scattering cross section for the F centre in CsBr, which exhibits similar complex structure due to spin–orbit and Jahn–Teller active electron–phonon interactions [10] and shows that these may not be completely neglected.

With regard to the dependence on excitation photon energy, in CsBr the Raman spectra behave basically like the infrared vibrational emission [4]. Depending to some extent on CN^- concentration, the infrared emisson spectra exhibit four (or sometimes even five) $\Delta v = -1$ transition for excitation with $F_H(1)$ light, but consist of merely three lines for $F_H(2)$ excitation. This very characteristic distinction is also obvious from the excitation spectra of the various infrared luminescence lines, which show peaks at the $F_H(1)$ and $F_H(2)$ band maxima for the $v = 3 \rightarrow 2$ emission line, but contain only one peak (at the $F_H(1)$ maximum) in the case of the $v = 4 \rightarrow 3$ transition. The Raman and infrared results in CsBr are quite different from those in CsCl, where in both techniques $F_H(1)$ and $F_H(2)$ excitations give rise to identical distributions of population in the excited CN^- vibrational states.

Concerning the electronic relaxation process and the electronic–vibrational energy transfer mechanism, the observed difference in the number of Raman lines suggests two possible interpretations:

(i) $F_H(1)$ and $F_H(2)$ excitations entail different relaxed excited states and hence distinctly different transfer pathways.

(ii) Excitation with $F_H(1)$ and $F_H(2)$ light results in identical relaxed excited states but, owing to the difference in electron/CN^- vibrational coupling strengths, transfer

and F-centre/lattice relaxation proceed on different timescales for the two excitations, finally resulting in the observed variations in Raman intensity distribution.

The available results do not yet permit one to decide between these alternatives. Assuming tentatively the second one to apply, figure 4 shows that, contrary to the strength of the corresponding absorption coefficients (see figure 1), the Raman intensities for all anti-Stokes lines are larger for $F_H(1)$ than for $F_H(2)$ light, suggesting the electron/CN^- vibrational coupling to be stronger for $F_H(1)$ excitation (excited electronic p state parallel to the $F_H(CN^-)$ centre and CN^- molecule axes). In this case one therefore expects, subsequent to the absorption process, energy transfer faster than (perturbed) F-centre relaxation into the relaxed excited state, so that transfer already occurs in the course of the relaxation process close to the unrelaxed situation. In complete agreement with the experimental findings, from the energy position of the $F_H(1)$ absorption (with an estimated zero-phonon energy of about 1.6 eV, which determines the energy difference between the unrelaxed electronic ground and excited states of the defect centre) a maximum of six Raman lines is expected, corresponding to a total vibrational energy of 1.49 eV. The weaker coupling for $F_H(2)$ excitation (excited p states perpendicular to the centre axis) on the other hand results in a relatively slower energy transfer into vibrational states taking place when the system is close to its relaxed excited state. Although the electronic luminescence of the $F_H(CN^-)$ centre seems to be completely quenched and therefore the energies of the relaxed electronic states are unknown, it is reasonable from the expected Stokes shift (emission band of unperturbed F centre in CsBr at 0.91 eV [11]) that any number of Raman lines smaller than six may be produced in this situation, which is again in agreement with the experiment. Nevertheless, alternative (i) cannot be excluded at present.

3.3. Polarisation of spectra

Examples of polarised resonant Raman Stokes and anti-Stokes spectra excited in the $F_H(1)$ and $F_H(2)$ absorption bands are illustrated in figures 5 and 6, with the polarisations of the incident and scattered light represented in the usual notation (e.g. [1 1 0][1 1 0]). As described above, the spectra may be considered to originate from a two-step process in which one photon is used, via electronic–vibrational energy transfer, to populate higher vibrational states, while a second one probes this population in a Raman scattering event. While vibrational emission measures the population of excited vibrational states directly and hence in principle reflects the polarised excitation and subsequent energy transfer, the Raman spectra are certainly affected by additional selection rules combined with resonant enhancement of line intensities, leading altogether to a quite different appearance.

Pursuing this idea of a two-step process, the CN^- ion is regarded as a ⟨1 0 0⟩-oriented vibrating system independent of which of the $F_H(CN^-)$ optical transitions the vibrational states are being excited through. From the orientation of the polarisability tensor, which is then assumed to transform according to the Raman-allowed irreducible representations of the host crystal O_h point symmetry, we expect only A_{1g} and E_g scattering, while no T_{2g} contribution to the Raman line should occur [7]. The experimental data displayed in figures 5 and 6 do not fully confirm this prediction. The [0 0 1][1 $\bar{1}$ 0] polarised spectrum, which only contains a T_{2g} component ($\frac{1}{2}T_{2g}$), rather shows substantial intensity, although smaller compared to the ($A_{1g} + \frac{1}{4}E_g + \frac{1}{2}T_{2g}$) and $\frac{3}{4}E_g$ spectra obtained for [1 1 0][1 1 0] and [1 1 0][1 $\bar{1}$ 0] polarisations, respectively. The same result was found in a

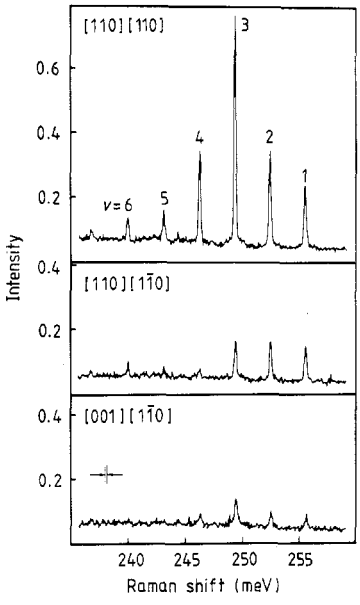

Figure 5. Polarised anti-Stokes Raman spectra of $F_H(CN^-)$ centres for $F_H(1)$ excitation at $T = 20$ K. Excitation at 1.800 eV with 180 mW. The polarisation vectors of the incident and scattered light are as indicated. The intensities are true to scale and comparable with those in figure 6.

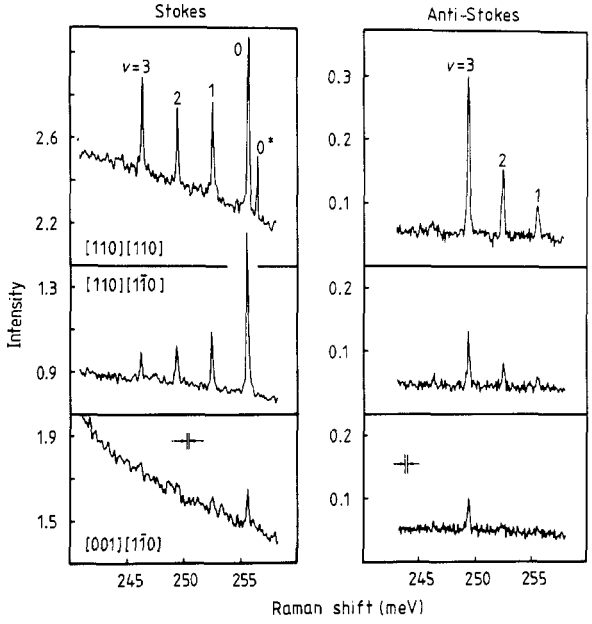

Figure 6. Polarised Stokes (left) and anti-Stokes (right) Raman spectra of $F_H(CN^-)$ centres for $F_H(2)$ excitation at $T = 20$ K. Excitations are at 1.980 and 1.960 eV, respectively, with 180 mW. The polarisation vectors of the incident and scattered light are as indicated. The intensities are true to scale and are comparable with those in figure 5. The line marked by * corresponds to a Stokes transition $v = 0 \rightarrow 1$ of unperturbed ('free') CN^-. Note subtraction of background in all Stokes spectra.

⟨100⟩-oriented sample. It again showed a non-negligible T_{2g} component (in [100][010] geometry), which amounts to about 10% of the $(A_{1g} + E_g)$ component observed in [100][100] geometry. In both CsCl and CsBr, deviations from the behaviour expected for a strictly ⟨100⟩-oriented $F_H(CN^-)$ centre were previously found in polarised vibrational emission [1, 4] following polarised $F_H(2)$ excitation. This probably suggests a modified defect structure, which will certainly affect the Raman result. An additional complication is noticed from the comparison of the Raman spectra (at fixed excitation) in different geometries (compare e.g. the [110][110] with the [110][1$\bar{1}$0] polarised spectra in figure 5 or in figure 6 (left)). For corresponding lines in these spectra the intensity ratio is found to vary substantially, also indicating a more complex polarisation behaviour.

We note two additional observations in the Stokes spectra of figure 6 (left):

(i) The occurrence of an intense polarisation-dependent background underlying the narrow Raman lines (note suppression of zero point of intensity), which is quite common for Raman scattering of F-type centres. It rises strongly with increasing excitation photon energies above 1.95 eV. For excitation at around 2 eV, we found a pronounced peak of

this emission at 1.8 eV, but did not investigate systematically if it is correlated with the $F_H(CN^-)$ or a different defect centre.

(ii) An additional narrow Raman line emerges in the [1 1 0][1 1 0] polarised spectrum on the high-energy side at 256.3 meV. From its energetic position (see table 1) this line is readily interpreted as due to Raman scattering from isolated ('free') CN^- defects [12]. Upon closer inspection, it is realised that the dominant intensity of this line appears in A_{1g} symmetry, while no intensity at all is observed in the E_g spectrum ([1 1 0][1 $\bar{1}$ 0]), the overall T_{2g} component ([0 0 1][1 $\bar{1}$ 0]) being weak anyhow. This polarisation behaviour, which we have studied in independent measurements not reported here, is consistent with the ⟨1 1 1⟩ orientation of unperturbed CN^- previously suggested for caesium halides [12]. The assignment is supported by the fact that the only Raman transition observed is the one with the vibrational ground state as initial state ($v = 0 \rightarrow 1$), the lack of any other Stokes and anti-Stokes transitions of this species proving that higher vibrational states are not occupied. In contrast to the F-centre/CN^- aggregated ($F_H(CN^-)$) pair, for isolated CN^- (electronic) excitation cannot be accomplished by visible light, since its electronic transitions are in the ultraviolet [13]. Population of higher vibrational states (via direct electronic–vibrational coupling) is therefore impossible, leaving the $v = 0$ state the only state populated.

The non-resonant excitation explains why this line is considerably less intense in comparison with the $v = 0 \rightarrow 1$ transition (at 255.5 meV) for the $F_H(CN^-)$ complex although the concentration of isolated CN^- molecules is much larger than the $F_H(CN^-)$ concentration. Assuming (from the absorption strength) an $F_H(CN^-)$ centre concentration of 10^{17} cm^{-3} and 10^{19}–10^{20} isolated CN^- molecules per cm^3 in our sample, from the ratio of integrated intensities of the two lines we estimate a resonance enhancement factor of about 10^3.

3.4. Dependence on excitation power and temperature

Important parameters that affect the spectra are excitation power and crystal temperature. Corresponding to the two-step nature of the process that produces the Raman spectra and includes (i) population of excited CN^- vibrational states followed by (ii) scattering from these, a quadratic dependence of anti-Stokes intensities on exciting laser power (P_L) can be expected. We investigated this dependence for either $F_H(1)$ or $F_H(2)$ excitation by varying P_L over a fairly wide range between 2 and 300 mW. As illustrated in figure 7 for $F_H(2)$ excitation, the result is in excellent agreement with this expectation at the lowest pumping powers (2–10 mW) we could use to obtain sufficiently good Raman signals. Already at about 10 mW, depending on temperature, the line intensities show deviations from this behaviour, which are different for the various Raman transitions. For example, under $F_H(1)$ excitation at 20 K (figure 8) we find in the range 10–20 mW a dependence of scattered intensity on P_L less than quadratic but superlinear for all lines except for $v = 6 \rightarrow 5$, which varies linearly. At still stronger excitation (50–300 mW), the intensities of lines from higher states ($v = 6 \rightarrow 5$, $5 \rightarrow 4$, $4 \rightarrow 3$) start to become saturated, while those involving lower levels ($v = 3 \rightarrow 2$, $2 \rightarrow 1$, $1 \rightarrow 0$) still increase, with the $3 \rightarrow 2$ line remaining strongest at all powers. At the highest power used, the $v = 2 \rightarrow 1$ and $1 \rightarrow 0$ transitions become even more intense than the $4 \rightarrow 3$ line, implying a relatively stronger decay of higher states and redistribution of occupation in favour of lower vibrational levels.

We consider this complex behaviour to originate from two counteracting effects caused by the increase in laser power. Increasing power not only raises population but

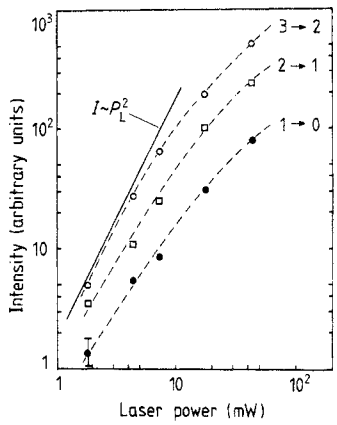

Figure 7. Dependence of integrated anti-Stokes Raman intensities on laser power in the low-power regime. The spectra are excited in the $F_H(2)$ band at 1.980 eV at $T = 5$ K. The full line corresponds to the expected $I \sim P_L^2$ dependence in the double-logarithmic plot.

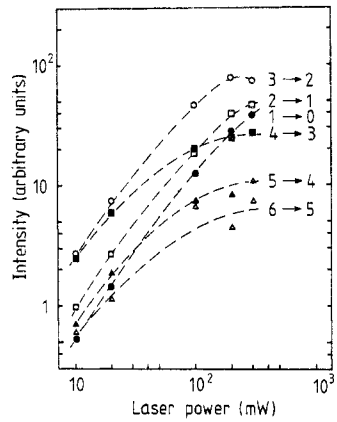

Figure 8. Dependence of integrated anti-Stokes Raman intensities on laser power in the high-power regime. The spectra were excited in the $F_H(1)$ band at 1.787 eV at $T = 20$ K. The lines are guidelines for the eye.

obviously, at high power levels, results in local heating, reducing the total vibrational lifetime due to the growing importance of non-radiative processes ($\tau_{tot}^{-1}(T) = \tau_{rad}^{-1} + \tau_{non\text{-}rad}^{-1}(T)$). Under continuous excitation, the occupation number of vibrational state v is given by $N_v \sim P_L \tau_v$ (τ_v = total lifetime of this state), resulting in the intensity for an anti-Stokes transition from this state $I_{v\to(v-1)} \sim P_L N_v \sim P_L^2 \tau_v$. Consistent with the experimental finding, this expression qualitatively describes the observed power dependence: at low excitation levels when τ_v = const., the intensity is quadratic in laser power, while the reduction of τ_v by temperature explains the deviation from this behaviour at higher powers. Since the lifetimes of the various vibrational states will be affected differently by temperature, altogether this leads to the observed complex intensity variations.

To separate the temperature effect on the vibrational states we measured the anti-Stokes spectra as a function of temperature at constant excitation power. For $F_H(1)$ and $F_H(2)$ excitations we found qualitatively the same behaviour as shown in figures 9 and 10, with only slight differences due to the different excitation powers used (170 and 45 mW, respectively). With increasing temperature, the overall integrated intensity gradually reduces with a relatively steeper decrease for most lines above 30–50 K. Concomitantly a redistribution of occupation among the vibrational states is observed, implying preferential depopulation of the higher quantum states in favour of the lower ones, again in agreement with the expected temperature dependence of τ_v.

The (relative) occupation number N_v of a vibrational quantum state v can be evaluated from the measured Raman intensities I_v by using the relations [14]

$$N_v \sim I_{v\to(v+1)}/E_S^3(v+1) \qquad \text{for Stokes processes}$$

and

$$N_v \sim I_{v\to(v-1)}/E_{AS}^3 v \qquad \text{for anti-Stokes processes.}$$

Here v labels the initial vibrational state for each process, and E_S and E_{AS} are the Stokes

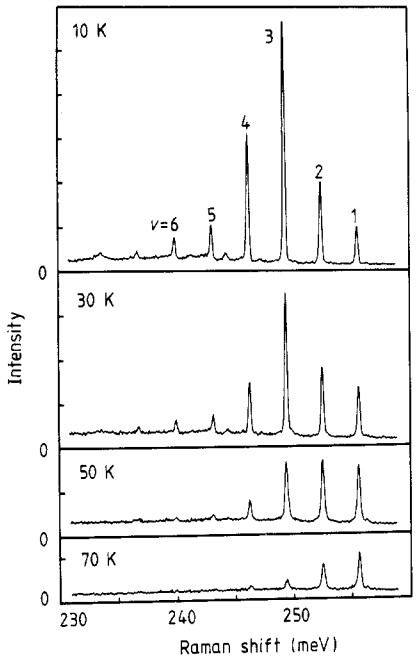

Figure 9. Anti-Stokes Raman spectra at different temperatures obtained under 1.793 eV ($F_H(1)$) excitation with 170 mW.

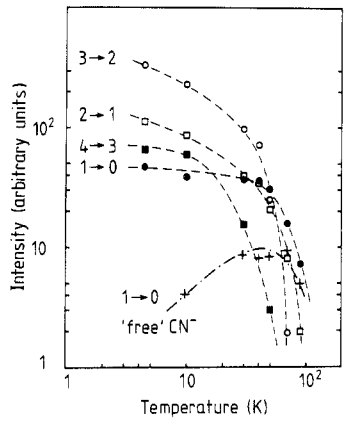

Figure 10. Temperature dependence of anti-Stokes Raman line intensities obtained under 1.950 eV ($F_H(2)$) excitation with 45 mW. The crosses mark the $v = 1 \rightarrow 0$ transition of isolated ('free') CN^-.

and anti-Stokes scattered photon energies, respectively. Since experimentally we were counting photons $n \sim I/E$, we use the third instead of fourth power of energies in the denominator. The expressions show that, different from infrared vibrational emission, the Raman spectra do not directly image the relative population of states. The dominant effect in computing N_v from the measured intensities stems from the factors $(v + 1)$ and v in the denominator. Relative to the Raman intensity distribution, the population of states with larger v is suppressed compared to that with smaller v. We find from analysing the Stokes spectra that the vibrational ground state ($v = 0$) is populated strongest under all excitation conditions used. This is directly evident from figures 2 and 6, where the Stokes $v = 0 \rightarrow 1$ transition occurs most intensely while all other transitions in the spectra have to be reduced in strength by $(v + 1)$ to represent the relative magnitude of N_v for higher vibrational states. Moreover we establish from the intensity distribution in both Stokes and anti-Stokes spectra that the $v = 3$ state, although much less populated than the vibrational ground state ($v = 0$), is inverted or at least comparable in population with respect to $v = 2$, i.e. $N_3 \geq N_2$. If the temperatures are not too high ($T \leq 20$ K), this holds good for nearly the whole power range covered by our experiments (see e.g. the anti-Stokes spectra in figures 2 and 3 for $F_H(2)$ and $F_H(1)$ excitation). To give representative numbers, for a sample excited with $P_L = 45$ mW in the $F_H(2)$ band ($T =$ 4.5 K) we calculate that about 90% of all centres are in the vibrational ground state, while 3% and 4% are in the $v = 2$ and $v = 3$ states, respectively, with the remainder in $v = 1$. Using higher laser power ($P_L = 180$ mW) in a different sample (at $T = 20$ K), the corresponding numbers are 68%, 7% and 7%, respectively. The results show that

$F_H(CN^-)$ centres in the host CsBr, like in CsCl, are potential candidates for laser applications. Although the highly efficient energy transfer observed in CsCl [1] in this respect makes this material a very promising system, and infrared superfluorescence and first laser oscillation have already been observed [15, 16] in practice CsBr might have the advantage of easier crystal growth and additive colouration.

Regarding the effect of temperature on the resonant Raman spectra, we mention one more experimental observation, which has been made before in the pulsed Raman measurements in CsCl [5]. Upon raising the temperature (see figure 10), we find in the anti-Stokes spectrum a tiny but clearly discernible $v = 1 \rightarrow 0$ transition (at 256.3 meV) due to isolated ('free') CN^- growing in intensity relative to the corresponding Raman line of the F-centre/CN^- coupled defect pair. As known from infrared vibrational emission [1, 4], at relatively high concentration of CN^- (10^{-2}, say) energy may be transferred from vibrationally excited $F_H(CN^-)$ centres to isolated CN^- molecules. This transfer should be most efficient between the $v = 1$ states which, in comparison to higher vibrational states, have long lifetime and minimum energetic difference. The energy barrier between the two states is 0.8 meV (see table 1), so that thermal energy is needed to achieve population of the $v = 1$ state of isolated CN^-. This is the effect we observe for $T > 40$ K, the temperature dependence of the intensity ratio of the two lines being roughly consistent with their energetic distance. In comparison with infrared vibrational emission, where thermally activated vibrational energy transfer leads to much more intense emission from isolated CN^-, in anti-Stokes Raman scattering the process related to the F-centre/CN^- coupled pair dominates because of resonance enhancement.

4. Concluding comments and outlook

The strength of Raman signals observed for excitation in either absorption component, which in spite of smaller absorption is considerably larger for $F_H(1)$ than for $F_H(2)$ excitation, suggests that the energy transfer occurs with the F centre in its excited state and obviously depends on the orientation of its electronic p wavefunction. Since the energy transfer with regard to the lattice vibrations proceeds in a non-equilibrium state, it may be considered as 'hot transfer', which had previously been discussed between electronic states of defect centres [17]. It is characterised by the fact that no energy loss takes place after photo-excitation and prior to transfer, so that the absorption spectra of the 'donor' and the 'acceptor' overlap. For hot transfer to occur, the donor–acceptor spacing has to be small, a requirement fulfilled in the present case since the donor (F centre) and the acceptor (CN^-) actually form a close pair. Moreover, its efficiency depends on the relative orientation of the interacting transition dipole moments, which qualitatively would account for the observed difference in Raman signal strengths under $F_H(1)$ and $F_H(2)$ light excitation (F-centre transition moment parallel and perpendicular to CN^- vibrational moment, respectively). In the case of the $F_H(CN^-)$ centre, however, the transfer process clearly differs from the case above in that electronic energy transforms into CN^- internal vibrational energy. Owing to the difference in quantum energies, this can occur through a higher-order process only, which would give rise to an extremely weak absorption of the acceptor and hence inefficient energy transfer. To explain the efficiency of the transfer, one may therefore have to take into account the possibility that the excited F electron strongly influences the CN^- excited electronic states, which, in a simple band structure picture, are situated near the conduction band edge and close in energy to the excited state of the F centre. This would allow the energy transfer to

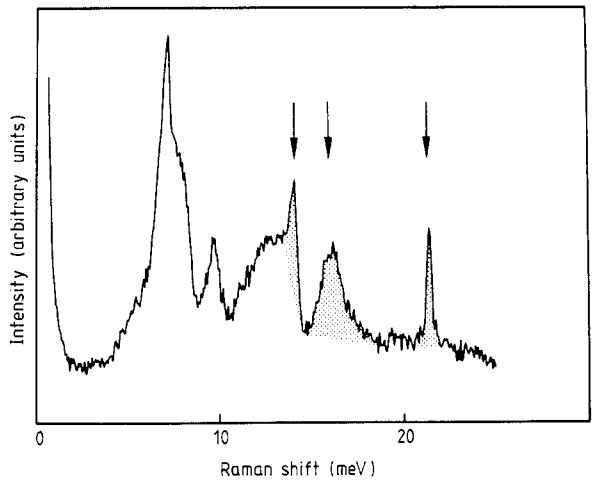

Figure 11. Low-energy resonant Raman spectrum of $F_H(CN^-)$ centres showing the defect interaction with the perturbed lattice phonon spectrum. The arrows mark additional features appearing after F-centre/CN^- aggregation. The spectrum is unpolarised and excited in the $F_H(1)$ absorption at 1.785 eV with 70 mW at $T = 5$ K.

proceed through this excited state, with the transformation of electronic into vibrational energy being accomplished by electronic-vibrational coupling within this 'new' defect centre. Since in the Raman experiments the vibrational excitations in the electronic ground state are probed, the interaction of the excited F-centre/CN^- molecule electronic states will have no effect on the Raman transition energies, but may lead to appreciable changes in stretching-mode energy in the excited electronic state.

Additional knowledge necessary for a complete understanding of the F-centre/CN^- pair properties can be expected from the interaction of the defect with the surrounding CsBr lattice and from the local-mode spectrum reflecting the effect of $Br^- \rightarrow CN^-$ substitution. This information is contained in the low-energy resonant Raman spectrum, which is presently under study. A preliminary result is illustrated in figure 11, showing this spectrum in the 0–25 meV range. Most of the spectral features with regard to energy positions and polarisation properties (not shown) correspond to first-order Raman scattering known for isolated F centres in CsBr [10], with the highest (LO(Γ)) energy at 13.9 meV [18]. Following F-centre/CN^- aggregation, close to and beyond the LO(Γ) lattice phonon energy three additional peaks emerge at 13.9, 15.9 and 21.2 meV. The 15.9 meV line is distinctly different in width and shape from the other two and also appears as a weak replica on the low-energy side of several of the CN^- anti-Stokes vibrational lines (e.g. L_3, L_4 in figure 3). The origin of these additional Raman transitions is not clear and certainly cannot be explained by only local-mode excitations induced by the mass change that accompanies the replacement of Br^- by CN^-. First measurements have shown an interesting dependence on excitation photon energy across the $F_H(CN^-)$ absorption and on light polarisation. These dependences are presently under study and certainly will reveal further details of the defect structure. In particular, we plan to study higher-order scattering, which provides detailed information on the local dynamics and vibronic interaction of the defect. The occurrence of three additional peaks in the perturbed phonon Raman spectrum already seems to point towards a centre with a greater complexity than the model discussed above, for which only two local-mode components would be predicted. This necessity for a model refinement, already encountered in the context of the Raman results for the CN^- internal vibration, certainly requires further investigations.

Acknowledgment

Support for this work by the Deutsche Forschungsgemeinschaft and for one of us (FL) by the National Science Foundation is greatly appreciated.

References

[1] Yang Y, von der Osten W and Lüty F 1985 *Phys. Rev.* B **32** 2724
[2] Lüty F 1968 *Physics of Color Centers* ed. W B Fowler (New York: Academic) p 181
[3] Yang Y and Lüty F 1983 *Phys. Rev. Lett.* **51** 419
[4] Yang Y and Lüty F 1986 unpublished
[5] Tsen K T, Halama G and Lüty F 1987 *Phys. Rev.* B **36** 9247
[6] Henry C H and Slichter C P 1968 *Physics of Color Centers* ed. W B Fowler (New York: Academic) p 351
[7] Hayes W and Loudon R 1978 *Scattering of Light by Crystals* (New York: Wiley)
[8] Karplus M and Porter R N 1970 *Atoms and Molecules* (London: W A Benjamin)
[9] Lüty F 1985 *Cryst. Latt. Defects Amorph. Mater.* **12** 343
[10] Mulazzi E and Buisson J P 1978 *Proc. Int. Conf. Lattice Dynamics* ed. M Balkanski (Paris: Flammarion) p 220
[11] Lynch D W, Brothers A D and Robinson D A 1975 *Phys. Rev.* A **139** 285
[12] von der Osten W and Lüty F 1987 *Phys. Rev.* B **35** 7684
[13] von der Heyden E and Fischer F 1975 *Phys. Status Solidi* b **69** 63
[14] Koningstein J A 1972 *Introduction to the Theory of the Raman Effect* (Dordrecht: Reidel)
[15] Gellermann W, Yang Y and Lüty F 1986 *Opt. Commun.* **57** 196
[16] Yang Y and Lüty F 1988 *J. Luminesc.* **40** & **41** 565
[17] Tekhver I Yu and Khizhnyakov V V 1975 *Sov. Phys.–JETP* **42** 305
[18] Rolandson S and Raunio G 1971 *Phys. Rev.* B **4** 4617